Mon. Not. R. Astron. Soc. **327,** 1288–1296 (2001)

Short period line profile and light variations in the Be star ω Orionis

L. A. Balona,[1★] C. Aerts,[2] H. Božić,[3] E. F. Guinan,[4] G. Handler,[1] D. J. James,[5,6] A. B. Kaye[7]† and R. R. Shobbrook[8]

[1]*South African Astronomical Observatory, PO Box 9, Observatory 7935, Cape Town, South Africa*
[2]*Instituut voor Sterrenkunde, Katholieke Universiteit Leuven, Leuven, Belgium*
[3]*Hvar Observatory, Faculty of Geodesy, Zagreb University, Kačićeva 26, 10000 Zagreb, Croatia*
[4]*Astronomy and Astrophysics Department, Villanova University, Villanova, PA 19085, USA*
[5]*School of Physics and Astronomy, University of St. Andrews, North Haugh, St. Andrews, Fife KY16 9SS*
[6]*Observatoire de Genève, Chemin des Maillettes, No. 51, CH-1290 Sauverny, Switzerland*
[7]*Applied Physics Division, X-5, Los Alamos National Laboratory, USA*
[8]*Research School of Astronomy and Astrophysics, Australian National University, Canberra, ACT, Australia*

Accepted 2001 July 13. Received 2001 July 13; in original form 2001 March 23

ABSTRACT

We present the results of a multisite spectroscopic and photometric campaign on the Be star ω Orionis. From the photometry and radial velocity variation of several spectral lines, we confirm that the star is a variable with period $P = 0.97$ d. Only one period can be extracted from both the photometric and radial velocity observations. We find that the projected rotational velocity from the helium lines ($v \sin i = 173\,\mathrm{km\,s^{-1}}$) is considerably smaller than from the metal lines ($v \sin i = 226\,\mathrm{km\,s^{-1}}$). The line profiles show an excess absorption feature moving from blue to red for half the period and from red to blue for the other half of the period. Another excess absorption feature moves exactly out of phase. The excess absorption features are present in photospheric lines as well as in lines which are significantly affected by circumstellar material, such as Hβ. From this we conclude that the periodic variations are most probably associated with corotating circumstellar material.

Key words: line: profiles – stars: early-type – stars: emission-line, Be – stars: individual: ω Ori.

1 INTRODUCTION

The mechanism which is responsible for mass loss in Be stars is not known. It is clear that rapid rotation plays an important role, since Be stars are more rapidly rotating than normal B-type stars of the same spectral type and luminosity class. However, rotation by itself is not a sufficient cause for mass loss, since most of the Be stars rotate at only 70 per cent of the critical rotational velocity (Porter 1996). Any theory which relies on accelerating material to the critical velocity at the equator cannot be reconciled with the observations. We also know that the mass ejection events episodically occur as 'outbursts', but we do not know what triggers such events.

The light and spectral line profiles of a large fraction of Be stars are known to vary with periods which closely correlate with the projected rotational velocity (Balona 1990, 1995). The periodic variability may provide an important clue to the mass-loss mechanism. Non-radial pulsation (NRP) has been proposed as a possible explanation. If mass ejection occurs in localized areas, one can expect the light and line profiles to vary with the period of rotation. This can occur either because the active region differs in temperature from the surrounding photosphere or because of obscuration by the emerging gas. Balona (1999) has argued that the line profile variations in some Be stars are too complex to be understood by NRP and suggests that the periodic variations are due to gas clouds corotating with the star.

A larger sample of Be stars is required in order to improve our understanding of the periodic variations. In order to study the mass-loss mechanism itself, we need to obtain time intensive sampling at high spectral resolution during an outburst. For this reason we decided to mount a campaign on ω Orionis (47 Ori, HR 1934, HD 37490, HIP 26594, B2 III). The star has a long history of irregular variability in Balmer line emission intensity. Hα was last in absorption in 1964. Since 1969, Hα emission has gradually increased in strength reaching a maximum ($E/C = 2.2$) in 1975. Because it has a small infrared excess and is located near nebulosity, ω Ori is frequently classified as a Herbig Be star (Hillenbrand et al. 1992; Thé, de Winter & Pérez 1994).

★E-mail: lab@saao.ac.za
†Visiting Astronomer, Kitt Peak National Observatory, National Optical Astronomy Observatories.

Table 1. Observing log for the spectroscopy. For each observatory, the Julian day, with respect to JD 245 1000, is shown for the first and last spectrum of ω Ori on the given night. N is the number of spectra obtained on that night and t the mean exposure time per spectrum in seconds.

Start	End	N	t	S/N	Start	End	N	t	S/N
	ESO					SAAO			
506.65	506.85	25	465	123	499.45	499.54	12	600	128
507.64	507.85	30	500	132	501.39	501.62	30	600	93
508.63	508.86	27	475	142	502.37	502.62	32	600	124
509.61	509.85	35	427	106	503.37	503.62	32	600	108
510.62	510.85	36	425	102	504.39	504.62	29	600	127
511.61	511.82	33	421	112	505.37	505.63	32	600	106
512.63	512.86	39	383	123	507.51	507.61	14	600	106
513.72	513.85	13	746	113	508.38	508.60	29	600	82
514.65	514.85	19	692	132	509.37	509.62	33	600	106
515.63	515.85	10	1740	130	510.38	510.62	32	600	98
516.64	516.85	9	1900	139	511.37	511.53	21	900	95
517.63	517.83	9	1900	128					
518.64	518.83	9	1811	148					
519.66	519.86	9	1789	145					
	KPNO					MSSSO			
Start	End	N	t	S/N	Start	End	N	t	S/N
512.64	512.96	9	1033	223	505.06	505.25	12	1004	132
513.68	513.89	2	1049	74	506.10	506.26	11	1077	134
514.71	514.98	9	1467	245	511.03	511.25	15	1050	142
515.70	515.94	7	1500	368	512.03	512.25	15	1050	112
516.70	517.02	11	1200	391					
517.69	518.04	15	1166	265					
518.66	519.05	20	1125	209					
519.82	520.07	4	1200	239					
520.80	520.83	2	1200	349					
521.79	522.04	4	2500	353					
522.76	523.04	3	2000	226					

The star is equatorially placed and is therefore suitable for observing from both hemispheres. The light curve has a period close to 1 d, requiring observations from different longitudes. Balona et al. (1987) found a photometric period of 0.96 d, or a double-wave period of twice this value, from observations at the South African Astronomical Observatory (SAAO) and the European Southern Observatory (ESO). This value was refined by further photometry from these two sites to obtain $P = 0.98078$ d (Balona, Cuypers & Marang 1992). Very few line profile observations have been obtained, and they are certainly not enough to confirm the photometric period. In this paper we present spectroscopic results from SAAO, Kitt Peak National Observatory (KPNO), ESO, and Mt. Stromlo and Siding Springs Observatory (MSSSO) and photometry from SAAO, Villanova, and Hvar.

2 OBSERVATIONS

Spectroscopic observations at SAAO were obtained using the GIRAFFE echelle fibre-fed spectrograph attached to the Cassegrain focus of the 1.9-m telescope. The GIRAFFE spectrograph has a resolving power of about 32 000. The 1024×1024 TEK CCD chip gives a dispersion of 0.06–0.09Å per pixel. A Th–Ar arc lamp was used for wavelength calibration with arc spectra taken at regular intervals to calibrate possible drifts. Flat-fielding was accomplished by illuminating the camera with uniform light using a tungsten filament lamp and a diffusing screen. The blaze correction was determined by measuring the response across each order when the fibre was illuminated by a tungsten lamp. The wavelength range was 4400–6680Å spread over 45 orders. Exposure times were normally 10 min for a S/N ratio of about 100. A total of 296 spectra of ω Ori was obtained (see Table 1) over a consecutive two-week period.

The spectroscopic observations in Chile were performed with the Swiss 1.2-m Ritchey-Chrétien Euler telescope at La Silla. Euler is equipped with a high-resolution echelle spectrograph, CORALIE, and a $2k \times 2k$ CCD camera with 15 μm pixels. The resolving power amounts to 50 000 and the total wavelength range is 3900–6800Å. The CORALIE spectra are extracted on-line following a standard echelle reduction procedure. The wavelength calibration is obtained by the use of a Th–Ar calibration lamp, whose spectra are simultaneously recorded in the sky orders. For a full description of the reduction scheme we refer to Baranne et al. (1996). The integration times were adapted to the atmospheric conditions and range from 6 to approximately 30 min. This ensured a S/N ratio of 100–150. In total, 303 spectra were obtained during two weeks.

The spectroscopic observations made at the MSSSO were obtained with the coudé echelle spectrograph on the Mt. Stromlo 1.9-m telescope during the period 1999 November 18–29. The observations were performed with a 31-line mm^{-1} echelle grating, a 2048×4096 pixel TEK CCD and a 1.2-arcsec slit, yielding a resolving power of about 40 000. The wavelength range obtained with this set up was 4500–6900Å spread over 42 orders. Exposure times were nominally $\simeq 18$ min for a S/N ratio of about 130. Owing to relatively inclement weather, a total of only 53 spectra of ω Ori was obtained (see Table 1) over a consecutive 12-d period. A Th–Ar arc lamp was used for wavelength calibration with arc spectra taken at regular intervals to calibrate possible drifts.

Flat-fielding was accomplished by illuminating the camera with uniform light using a tungsten filament lamp.

89 high S/N spectra were obtained over 12 nights at the KPNO during late 1999 November and early December (JD 2451512–2451523), with the 0.9-m coudé feed telescope and spectrograph. Each spectrum covers a wavelength range slightly larger than 300 Å centred on λ6566, and was obtained using grating A, camera 5, and the long collimator. Filter RG610 was used to block both higher and lower orders. Data were recorded on the F3KB CCD (3k × 1k pixels, 15 × 15 μm pixel size, 75 per cent DQE at 6560 Å). The typical exposure time for spectra in this region was 1200 s, resulting in a S/N of about 350. Th–Ar exposures used for wavelength calibration were taken immediately before and after each stellar exposure.

These spectra were reduced at the National Optical Astronomy Observatories NOAO offices in Tucson, Arizona in the standard fashion using IRAF[1] and included optimal aperture extraction, bias subtraction, and flat-field division.

In order to study the line profile variations, the continuum needs to be determined. Placing the continuum by hand is not an easy process. We preferred to rectify the spectra with the aid of a synthetic spectrum calculated using the SPECTRUM code (Gray & Corbally 1994). To do this, we calculated a synthetic spectrum covering the full echelle wavelength range using a Kurucz solar-abundance model atmosphere appropriate to a B2 III star ($T_{\rm eff} = 17000$, $\log g = 3.0$) and broadened with $v \sin i = 194\,{\rm km\,s^{-1}}$. To rectify the spectrum, each echelle order was divided by the synthetic spectrum and the result fitted with a third-order polynomial. Direct comparison of the rectified spectra with the synthetic spectrum showed that the above procedure is quick and effective.

Photometry was obtained using the Modular Photometer attached to the 0.5-m reflector of SAAO, Sutherland simultaneously with the echelle data at the same site. We used all four Strömgren *uvby* filters and the two local comparison stars, HR 1842 and 1871. All three stars were observed in sequence through a light neutral density filter. A total of 55 *uvby* observations were obtained over 10 nights between JD 245 1499.4 and 245 1511.5. The mean values from the literature for the two comparison stars are: HR 1842: $y = 5.443$, $b = 5.364$, $v = 5.375$, $u = 5.506$; HR 1871: $y = 6.566$, $b = 6.484$, $v = 6.496$, $u = 6.673$. The zero-points of our *uvby* observations were adjusted to give these values. The difference in magnitudes between the comparison stars closely matches the difference obtained from the above values to within the observational uncertainties (about 3 mmag).

A total of 79 *uvby* observations were obtained with the Villanova automatic telescope between JD 245 1473.0 and 245 1623.7 using HR 1872 (HD 36777, 38 Ori) as a comparison star. The adopted values are: $y = 5.346$, $b = 5.378$, $v = 5.566$, $u = 6.845$.

Photometric observations in the Johnson *UBV* system were obtained from the Hvar observatory, using HR 1842 as a comparison star and HR 1871 as a check star. A total of 64 observations were obtained. From all-sky photometry, the following values were derived for HR 1842: $V = 5.459$, $B = 5.282$, $U = 4.451$. Relative to this star, we find for HR 1871: $V = 6.585$, $B = 6.406$, $U = 5.611$. The standard error in these measurements is about 8 mmag, as derived from the scatter in the observations of HR 1871.

[1] IRAF is distributed by the NOAO, which is operated by the AURA, under contract to the National Science Foundation.

Because of poor weather, only 16 Johnson *BV* observations on two consecutive nights were obtained at the Siding Springs Observatory.

3 ROTATIONAL VELOCITY

We assume that the mean line profile of a large number of spectra is the best estimate of the photospheric line profile. In Figs 1 and 2 we show mean profiles of all measured lines for the SAAO and ESO data, which comprise the majority of spectra. The agreement in the line profiles is rather good except for Si III 4553 and Hβ. The discrepancy in the Hβ line is because of the difficulty in placing the continuum for such broad lines.

The projected rotational velocity of ω Ori was measured by Slettebak (1982) to be $160\,{\rm km\,s^{-1}}$. More recently, Ballereau, Chauville & Zorec (1995) found $v \sin i = 146\,{\rm km\,s^{-1}}$ by modelling

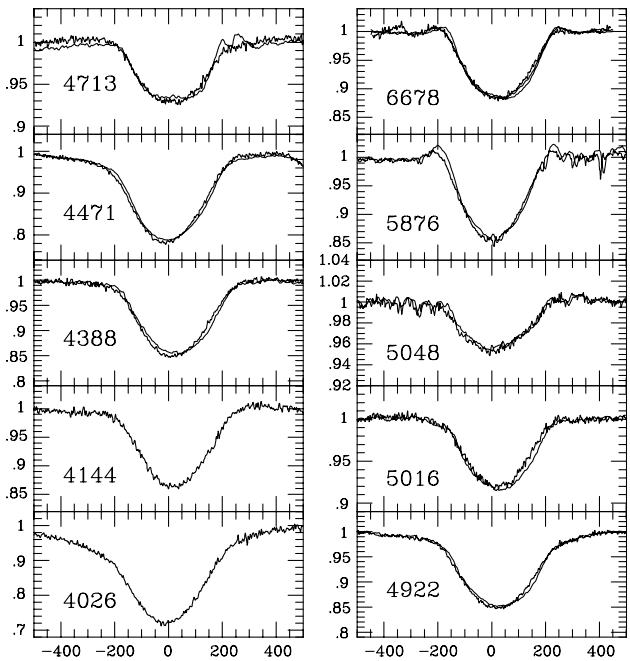

Figure 1. Mean rectified profiles of the helium lines for the SAAO data and the ESO data plotted on top of each other. The He I 6678 line also includes data from KPNO. The abscissa is in units of km s^{-1} as measured from the laboratory wavelength of the line.

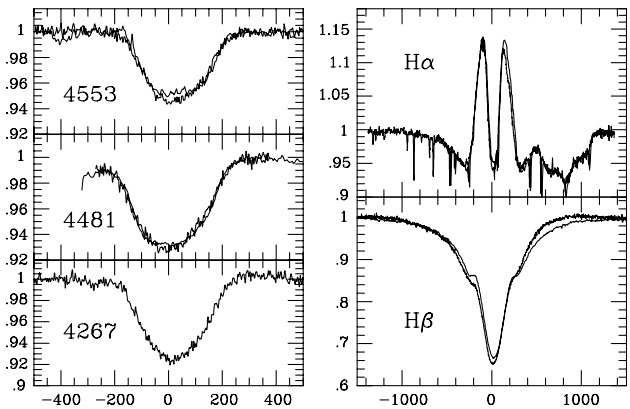

Figure 2. The same as Fig. 1 but for the C II 4267 line, the Mg II 4481, Si III 4553, 4567 and hydrogen lines.

the He I 4471 line. We determined $v \sin i$ from various helium and metal lines using the intrinsic line profile calculated from the SPECTRUM program and a non-linear least squares optimizing algorithm. For the rapid rotation seen in this star, the results are insensitive to the details of intrinsic line broadening. For example, we find $v \sin i = 183\,\mathrm{km\,s^{-1}}$ for He I 4922 (SAAO data) using the model intrinsic profile. Replacing the model profiles with a Gaussian profile of rms width 20 or $40\,\mathrm{km\,s^{-1}}$ both give $v \sin i = 188\,\mathrm{km\,s^{-1}}$, dropping to $v \sin i = 174\,\mathrm{km\,s^{-1}}$ only when the rms width is $80\,\mathrm{km\,s^{-1}}$. In contrast, the model intrinsic profile has an equivalent rms width of about $16\,\mathrm{km\,s^{-1}}$. Results are shown in Table 2.

The helium lines give significantly lower values than the metal lines. From all helium lines we obtain $v \sin i = 173 \pm 2\,\mathrm{km\,s^{-1}}$. For the metal lines (excluding one deviant SAAO measurement from Si III 4553) we find $v \sin i = 226 \pm 7$. In μ Cen (Balona et al. 2001) the metal lines give slightly higher values as well, but only by about $10\,\mathrm{km\,s^{-1}}$. The difference here is much larger. Some of the helium lines in ω Ori show wing emission (Fig. 1), particularly He I 5876 and He I 6678, arising from the circumstellar material. It is possible that all helium lines may be affected by the circumstellar material which could explain the smaller values of $v \sin i$ for the helium lines relative to the metal lines.

Table 2. Projected rotational velocity, $v \sin i$ ($\mathrm{km\,s^{-1}}$), obtained by non-linear least squares for various lines (laboratory wavelengths given). The standard deviation of the fit, σ, is in continuum units. For the helium lines, the range of fit was from -300 to $+300\,\mathrm{km^{-1}}$, while for the other lines it was from -150 to $+210\,\mathrm{km^{-1}}$. The column labelled RV is the radial velocity of the line ($\mathrm{km\,s^{-1}}$) as obtained from the fit. The last column is the equivalent width in Å.

Line	Season	$v \sin i$	σ	RV	EW
He I 4026.359	ESO	177	0.0072	6.0	1.45
He I 4143.761	ESO	173	0.0045	17.0	0.53
He I 4387.929	SAAO	179	0.0029	25.0	0.62
	ESO	169	0.0042	14.1	0.63
He I 4471.682	SAAO	174	0.0031	30.0	1.05
	ESO	174	0.0032	20.9	1.01
He I 4713.376	SAAO	175	0.0035	23.9	0.29
	ESO	180	0.0036	24.0	0.29
	MSSSO	184	0.0042	28.5	0.34
He I 4921.931	SAAO	183	0.0029	37.9	0.80
	ESO	181	0.0029	30.2	0.81
	MSSSO	184	0.0038	38.5	0.61
He I 5015.678	SAAO	171	0.0028	23.2	0.37
	ESO	168	0.0041	15.9	0.34
	MSSSO	180	0.0058	14.0	0.32
He I 5047.738	SAAO	171	0.0037	14.3	0.21
	ESO	175	0.0028	15.8	0.20
	MSSSO	173	0.0086	16.7	0.26
He I 5875.966	SAAO	159	0.0083	23.2	0.65
	ESO	158	0.0060	15.8	0.68
	MSSSO	152	0.0152	19.0	0.71
He I 6678.151	SAAO	172	0.0042	25.7	0.66
	ESO	168	0.0042	21.5	0.65
	KPNO	174	0.0036	27.5	0.66
	MSSSO	178	0.0079	19.9	0.99
All He lines			173 ± 2		
C II 4267.167	ESO	214	0.0032	22.5	0.28
Mg II 4481.228	SAAO	221	0.0023	14.7	0.30
	ESO	245	0.0029	13.7	0.31
Si III 4552.622	SAAO	157	0.0028	28.8	0.20
	ESO	223	0.0037	7.5	0.21
All metal lines			226 ± 7		

The *Hipparcos* parallax of ω Ori is 2.01 ± 0.94 mas. The uncertainty is too large to give a useful parallax which would be helpful in determining the radius. For a B3 star, Balona (1995) obtains $R/\mathrm{R}_\odot = 4.2$, 5.8 and 7.4 for classes V, IV and III, respectively. Porter (1996) finds a polar radius of 4.7 $R/\mathrm{R}_\odot$, $M/\mathrm{M}_\odot = 7.7$ and $V_{\rm crit} = 458\,\mathrm{km\,s^{-1}}$ for a B3 dwarf. Assuming $R/\mathrm{R}_\odot = 9 \pm 3$ for a B3 III star (allowing for an increase in radius caused by rotation) and taking $v \sin i = 200 \pm 30$ the longest period of rotation, assuming an inclination $i = 90°$, is $P = 2.3 \pm 0.8$ d.

4 THE PERIOD: PHOTOMETRY

The best photometric data set for a new period analysis is that obtained at SAAO. A total of 55 *uvby* data points was obtained over 12 nights. The Villanova data set comprises 79 data points, but is spread over 151 nights, while the Hvar data set comprises 64 points spread over 23 nights. In order to make use of all three data sets for period analysis, it is necessary to reduce them to a common standard. This is not very easy because a different comparison star is used for the Villanova observations, while the Hvar data are in Johnson *UBV*, not in *uvby*. Since the *V* and the *y* filters have very nearly the same effective wavelength, we decided to use this filter alone for the period analysis of the combined data. We adjusted the Hvar *V* data by -0.0175 mag to bring the *V* magnitudes of the two comparison stars to the same value as the SAAO adopted magnitudes, but left the Villanova magnitudes unchanged. Fourier periodograms of the *V* observations of these three data sets, separately and combined, are shown in Fig. 3. The amplitude of the combined data is much larger than that of the individual data sets because the period is so close to 1 d (each data set samples only a portion of the light curve).

The highest peak for the SAAO data set occurs at $f = 1.076 \pm 0.005\,\mathrm{cycles\,d^{-1}}$ in all four colours; no further significant periodicities are present. For the Villanova data set we find $f = 0.9455 \pm 0.0004\,\mathrm{cycles\,d^{-1}}$ for *y* and *b* or its 1-d alias $f = 1.0567 \pm 0.0004$ for *v* and *u* as the only significant period. The latter is not significantly different from the value found from SAAO. In the Hvar *UBV* data there is a peak at $0.224 \pm 0.002\,\mathrm{cycles\,d^{-1}}$. This peak and its 1-d alias appears in all three colours and appears to be a result of the time sampling, since the window function shows the same peak. Equally as strong, however, is a peak at $f = 1.049 \pm 0.002\,\mathrm{cycles\,d^{-1}}$.

Combining the SAAO and Villanova sets gives $f = 1.0026 \pm 0.0004$ and $1.0576 \pm 0.0005\,\mathrm{cycles\,d^{-1}}$ as the only two significant periods. The former frequency is probably an artefact arising from slight zero-point differences in the two data sets. Indeed, if we force the two data sets to give the same mean values in *uvby*, this frequency disappears from the periodogram. Combining the SAAO and Hvar data sets leads to $f = 1.0286 \pm 0.0004\,\mathrm{cycles\,d^{-1}}$ if one ignores the equally strong 0.224-cycles $\mathrm{d^{-1}}$ frequency (present only in the Hvar data). Combining all three *V* data sets gives $f = 1.0315 \pm 0.002\,\mathrm{cycles\,d^{-1}}$. Pre-whitening by this frequency leaves a pure noise spectrum. No other significant periodicities are present.

The formal errors in the frequency quoted here are from the formula by Kovacs (1981). The full width at half-maximum (FWHM) of the peaks in the periodograms are much larger than these errors (typically $0.05\,\mathrm{cycles\,d^{-1}}$). Considering the fact that the period is so close to 1 d, the probable systematic zero-point errors from different observatories, and the fact that Be stars show random variations on all time-scales, we believe that the formal

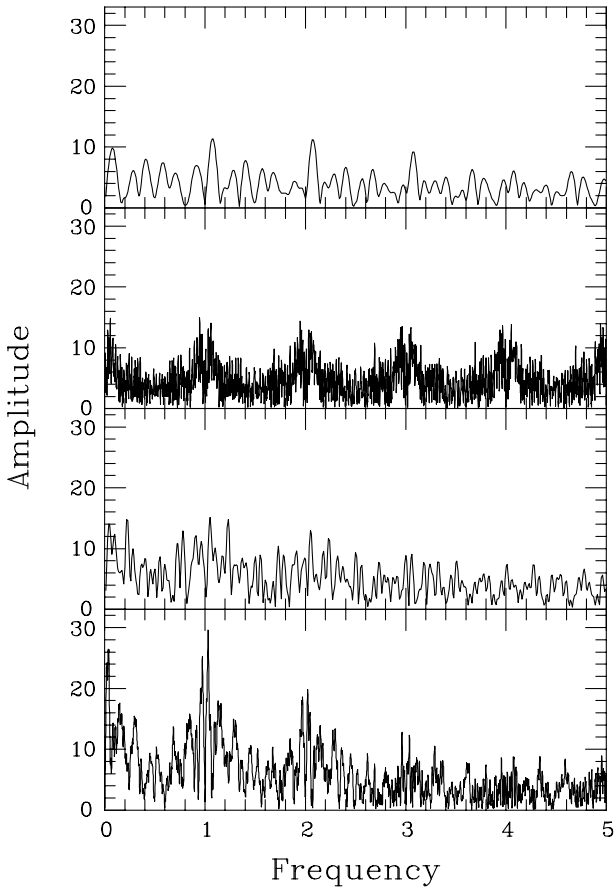

Figure 3. Fourier periodograms of Strömgren y or Johnson V photometry of ω Ori obtained in 2000. From top to bottom the panels show the periodograms of the SAAO data, the Villanova data, the Hvar data, and all three data sets combined. The frequency is in cycles d^{-1} and the amplitude in mmag.

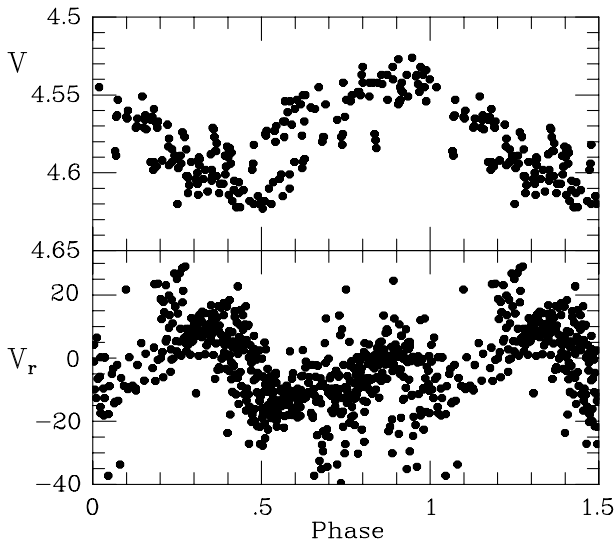

Figure 4. Phase diagrams for combined Strömgren y and Johnson V photometry (top panel) and radial velocities (helium triplets) of ω Ori. For the radial velocities, the mean velocity of each line was removed before averaging. The period $P = 0.97$ d and epoch of phase zero is JD 245 1000.000.

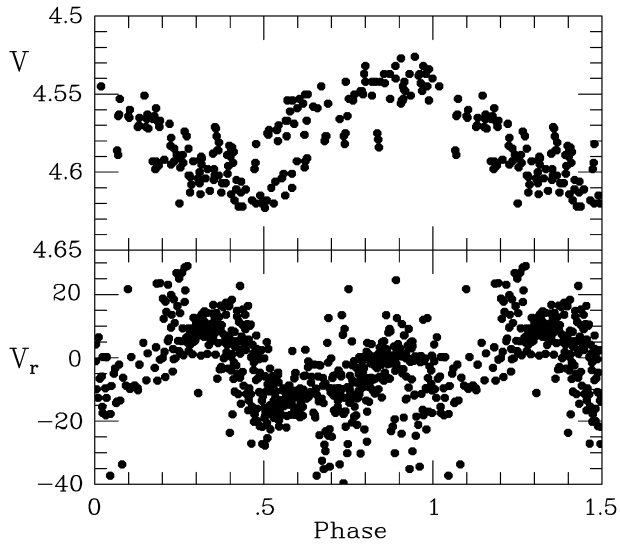

Figure 5. Phase diagrams for combined Strömgren y and Johnson V photometry (top panel) and radial velocities (helium triplets) of ω Ori. The period $P = 1.9389$ d and epoch of phase zero is JD 245 1000.000.

errors are too small and that the difference in frequencies between the various data sets are not significant. We therefore adopt the period which results when all three data sets are combined, $f = 1.03$ cycles d^{-1} with an uncertainty of about 0.01 cycles d^{-1} ($P = 0.97 \pm 0.01$ d) as the most probable value. This period is not significantly different from the period $P = 0.98$ d proposed by Balona et al. (1992).

The best-fitting Fourier curve has an amplitude of 0.010 ± 0.001 mag at this frequency. The light curve with the corresponding period is shown in Fig. 4 and with twice this period in Fig. 5. A considerable fraction of Be stars show a double-wave variation, but there is no strong reason to prefer the double-wave period for ω Ori on the basis of the phase diagrams. A phase dispersion minimization (PDM) analysis also confirms that there is no obvious preference for the double-wave solution.

The *Hipparcos* photometry is not sufficiently sampled to be of much use in determining the period. The star faded by about 0.06 mag during the 3 yr of observations. We removed this trend by fitting a parabola. The highest peak in the periodogram of the corrected photometry is at $f = 0.6807$ cycles d^{-1}, which bears no relationship to the frequency obtained from the ground-based data. The highest peak in the vicinity of one cycle d^{-1} is $f = 1.00658 \pm 0.00006$ cycle d^{-1}.

5 THE PERIOD: RADIAL VELOCITIES

We define the radial velocity as the position of minimum intensity of the line core relative to the laboratory wavelength of the line. Other definitions, such as the centroid of the line profile, can be adopted. The position of minimum intensity is more sensitive to changes in line profile, which is why it was chosen, but at the same time more prone to error. We measured this quantity by fitting a parabola to the pixels nearest to the line intensity minimum. The resulting value is dependent, to some extent, on the number of pixels used to define the parabola. In Table 3 we show the most probable frequency and radial velocity amplitude for the helium and metal lines in ω Ori. With three exceptions, the radial velocities confirm that the period of the star is close to 1 d.

In Fig. 6 we show the periodograms of helium triplets (He I 4471

Table 3. The most probable frequency (cycles d^{-1}) and amplitude (km s^{-1}) determined from the radial velocities of various lines in ω Ori. The source code is as follows: 1 – SAAO, 2 – ESO, 3 – MSSSO, 4 – KPNO. For Hα, results from the radial velocity of the central absorption dip (centre) and the blue and red emission wings are given.

Line	Source	Frequency	Amplitude
He I 4026.359	2	1.103	7.1 ± 0.6
He I 4143.761	2	0.531	5.5 ± 1.0
He I 4387.929	1+2	1.025	12.0 ± 1.3
He I 4471.682	1+2	1.065	8.3 ± 0.7
He I 4713.376	1+2+3	0.999	26.5 ± 2.4
He I 4921.931	1+2+3	1.021	12.1 ± 1.0
He I 5015.678	1+2+3	1.018	10.1 ± 1.4
He I 5047.738	1+2+3	0.920	9.7 ± 1.0
He I 5875.966	1+2+3	1.037	10.1 ± 0.7
He I 6678.151	1+2+3+4	1.034	14.4 ± 1.1
Hα – centre	1+2	1.084	5.0 ± 0.3
Hα – blue	1+2	0.487	2.5 ± 0.3
Hα – red	1+2	1.018	10.5 ± 0.3
Hβ	1+2	1.019	7.4 ± 0.5
C II 4267.167	2	0.515	4.8 ± 1.2
Mg II 4481.228	1+2	1.068	20.2 ± 1.5
Si III 4552.622	1+2	1.075	29.0 ± 1.9
He I singlets		1.023	13.5 ± 0.6
He I triplets		1.065	8.7 ± 0.6
Metals		1.074	26.3 ± 0.6

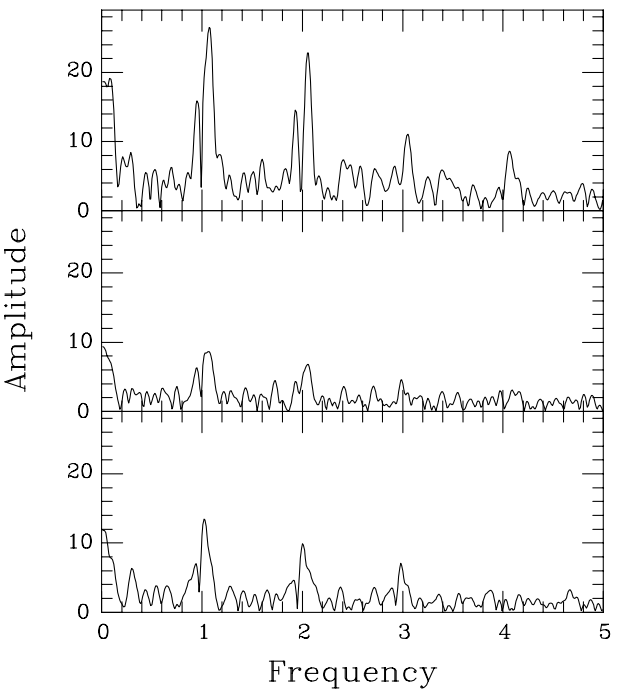

Figure 6. Periodograms of the radial velocities of metal lines (top panel), He I triplets (middle panel), and He I singlets (bottom panel). The frequency is in cycles d^{-1} and the amplitude in km s^{-1}.

and 5876), He singlets (He I 4922 and 6678) and metal lines (Mg II 4481 and Si III 4553). In Table 4 we show all significant frequencies present in these data. As in the photometry, we believe that the formal errors are probably too small. We need to assume a standard error of about 0.02 cycles d^{-1} to reconcile these frequencies. From the time range (24 d), we can expect a frequency resolution of no more than 0.04 cycles d^{-1}.

Table 4. List of all significant frequencies (cycles d^{-1}) and amplitudes (km s^{-1}) for the radial velocities of the He singlets, triplets and metal lines.

Frequency	Amplitude
He I singlets	
1.024 ± 0.001	13.6 ± 0.7
1.099 ± 0.004	6.1 ± 0.8
He I triplets	
1.068 ± 0.002	6.9 ± 0.6
1.023 ± 0.003	5.9 ± 0.6
1.723 ± 0.005	4.1 ± 0.5
0.941 ± 0.005	4.0 ± 0.5
Metals	
1.072 ± 0.001	22.9 ± 1.4
0.051 ± 0.004	11.9 ± 1.3

Table 5. Fourier parameters of the best-fitting sinusoid, $V_r = V_0 + A\cos 2\pi(t/P + \phi)$, to the Strömgren photometry, the radial velocity of the helium triplets, singlets, and the metal lines. The adopted period is $P =$ 0.97 d and the time, t, is measured with respect to JD 245 1000.000. The amplitude is in mmag or km s^{-1}. The rms error, σ, of the fit and the number of data points, N, are also shown. The mean radial velocity, V_0, is taken from Table 2.

Line	V_0	A	ϕ	σ	N
y	4.605 ± 0.001	12.7 ± 2	−0.47 ± 0.02	10.4	132
b	4.533 ± 0.001	14.0 ± 3	−0.46 ± 0.02	9.3	132
v	4.584 ± 0.001	10.5 ± 2	−0.47 ± 0.02	10.2	132
u	4.795 ± 0.001	13.6 ± 2	−0.49 ± 0.02	11.5	132
$b-y$	−0.071 ± 0.001	1.6 ± 1	−0.35 ± 0.09	5.5	132
$u-b$	0.261 ± 0.001	3.0 ± 1	0.26 ± 0.07	7.3	132
He Trip	22.6 ± 3.0	9.5 ± 0.6	−0.21 ± 0.01	10.6	589
He Sing	28.8 ± 3.5	13.5 ± 0.8	−0.29 ± 0.01	13.5	577
Metals	17.4 ± 3.7	22.5 ± 1.5	−0.16 ± 0.01	24.5	563

Figs 4 and 5 show the radial velocities from the helium triplet lines phased with the adopted photometric period $P = 0.97$ d and with twice this period. Since the radial velocities of individual triplet lines are systematically different, the mean radial velocity of each line was removed to give the mean radial velocity of the triplet shown in the figures. There is no apparent preference for a double-wave variation from the radial velocities. Table 4 shows the parameters of the best-fitting sinusoid for the helium triplets, singlets and the metal lines. The amplitude from the metal lines is about twice that of the helium lines. In Table 5 we show the Fourier parameters of the photometry and radial velocities with the adopted period of $P = 0.97$ d.

6 LINE PROFILE VARIATIONS

Because the line profile variations are small (less than 1 per cent of the continuum), they are difficult to detect when line profiles are directly plotted. The most convenient way to display the variations is to construct 'difference profiles' by dividing each line profile by the mean line profile. In this way, even small departures from the mean line profile can be visualized in a grey-scale diagram. By stacking difference spectra as a function of time in a grey-scale

image, the variation of the line profiles as a function of time can be easily seen. In stars such as η Cen (Balona 1999), μ Cen (Balona et al. 2001) and ϵ Cap (Balona & Lawson 2000), stacked difference spectra for each night usually show one or more moving absorption features characteristic of periodic Be stars.

We constructed phased grey-scale difference spectra for frequencies ranging from $f = 1.000$ to $1.070\,\mathrm{cycles\,d^{-1}}$ in steps of $0.002\,\mathrm{cycles\,d^{-1}}$ for the He I 4922 line. By visual inspection, we find that a range of possible periods around $P = 0.95$ d seem to give the most coherent grey-scale images. The adopted photometric period, $P = 0.97$ d, gives an image which is about as good as any other. In constructing the difference spectra, we divided each line profile by the mean line profile of the combined SAAO and ESO data. The mean residual absorption in the moving subfeatures is about 1 per cent of the continuum level in Si III 4553, He I 4922, He I 6678, and He I 5876. Rather than showing grey-scale images, the visibility of the moving features can be enhanced by extracting the first few minima of the difference spectra. A sample of these extracted minima for different spectral lines, phased with the photometric period, is shown in Fig. 7 using data from all observatories.

Because the period is so close to 1 d, data from any given site tend to cover a limited phase range. The data from ESO and SAAO, for example, barely overlap in phase. The KPNO data have the highest S/N and cover a longer time interval than the other data sets. Although of lower resolution than the other spectra, they provide a useful check on the reality of the phenomenon. In Fig. 8 we show the extracted minima of the residual absorption lines for the KPNO and MSSSO He I 6678 line. In Fig. 8 we also show the extracted minima for the Hβ line. The variations are almost as clear in Hβ as in some of the helium lines, although the core of the line is clearly formed in the circumstellar medium. The typical residual absorption depth in Hβ is about 2 per cent of the continuum.

Fig. 7 shows a residual absorption feature moving from blue to red from phases 0.9 to 0.4 and from red to blue between phases 0.4 and 0.9. At the same time, another strong absorption feature moves from blue to red between phases 0.4 and 0.9. A red to blue motion can occur when a corotating feature is seen over the pole in a star with moderate or low inclination. The limits of travel are confined to within about $\pm 200\,\mathrm{km\,s^{-1}}$, which is the projected rotational velocity. At phases 0.4 and 0.9 both features are visible on opposite limbs of the star. We may interpret the cause of the travelling residual absorption features as either because of NRP with $|m| = 2$ or as a result of diametrically opposed corotating clouds. As in many other Be stars, the pattern is visible in lines which are clearly affected by the circumstellar material such as He I 6678, He I 5876 and Hβ. For this reason, we believe that the variation is most likely due to corotating clouds.

To improve the S/N ratio, we averaged the SAAO and ESO line profiles for He I 4922 in phase bins of 0.05 periods, assuming the

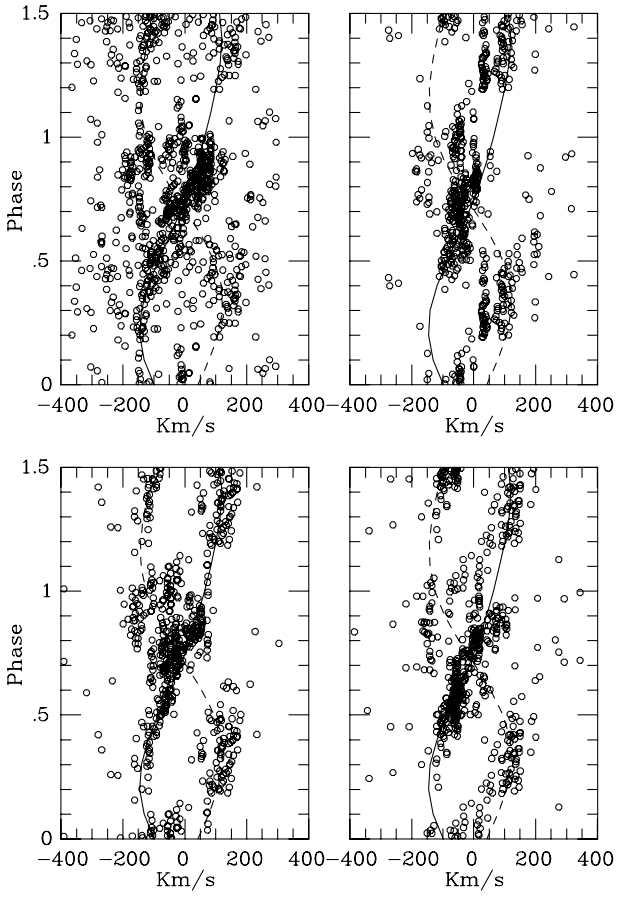

Figure 7. Extracted minima of excess absorption ridges are phased with $P = 0.97$ d. The epoch of phase zero is JD 245 1000.000. Top panel: left – Si III 4553, right – He I 5876. Bottom panel: left – He I 4388, right – He I 6678. The solid line indicates the general trend of the blue-to-red moving absorption subfeature and the dashed line the red-to-blue moving absorption subfeature.

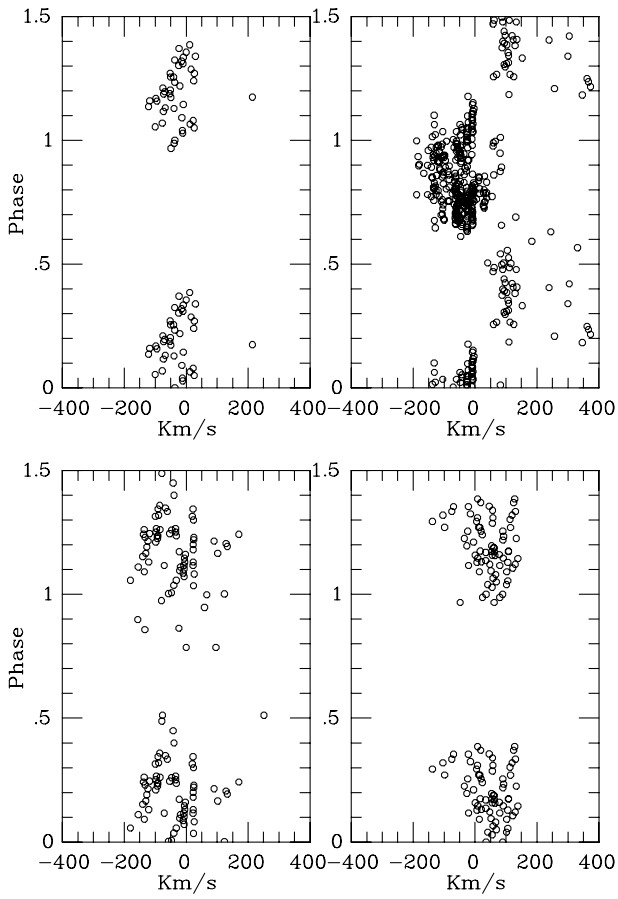

Figure 8. Extracted minima of excess absorption ridges are phased with $P = 0.97$ d. The epoch of phase zero is JD 245 1000.000. Top panel: left – MSSSO He I 4922, right – ESO and SAAO Hβ. Bottom panel: left – KPNO He I 6678, right – MSSSO He I 6678.

photometric period $P = 0.97$ d. In Fig. 9 we show the mean line profile as a function of phase. We divided each profile by the mean profile of all the SAAO and ESO data to generate the mean difference profile in phase bins of 0.05 periods. These are also shown in Fig. 9. In principle, it should be possible to model the line profile variations with NRP. There is a good chance that a suitable NRP model could be found to fit the data within the S/N ratio, since the variations are small. No doubt, a suitable model involving spot-like corotating clouds may also be found to fit the data. We did not pursue the idea of modelling the line profile variations because they are too small to be useful in discriminating between various models.

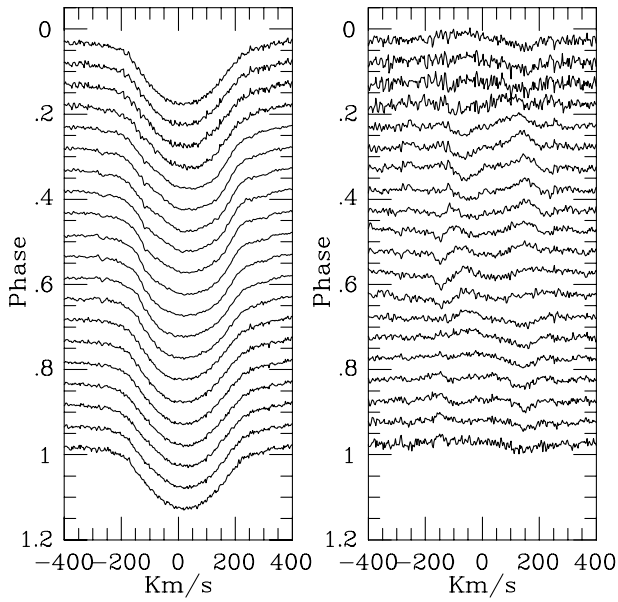

Figure 9. Left panel: the mean profile of the He I 4922 line for the ESO and SAAO data binned in units of 0.05 periods assuming $P = 0.97$ d. The epoch of phase zero is JD 245 1000.000. Right panel: the mean difference profile as a function of phase.

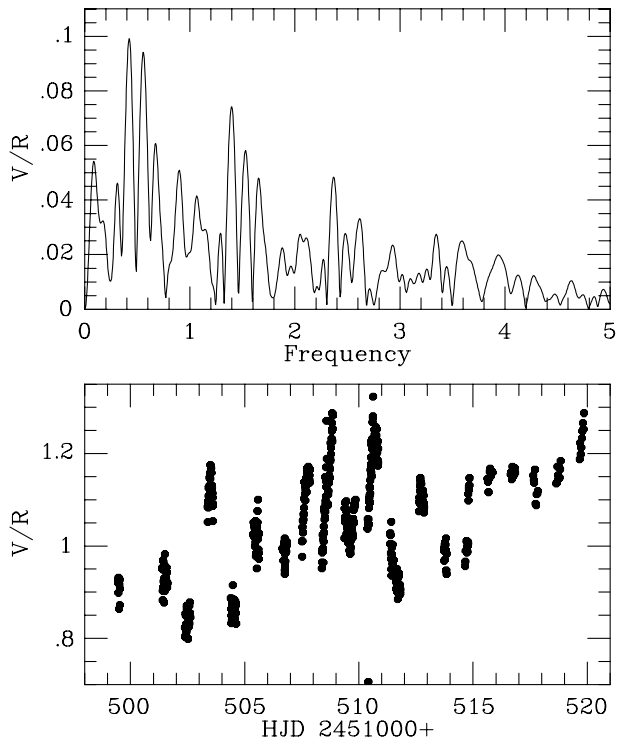

Figure 10. Bottom panel: the *VR* emission strength ratio for Hα as a function of time. Top panel: the periodogram of the *VR* ratio after the linear trend is removed. The frequency is in cycles d^{-1}.

The Hα line shows a central absorption flanked by two emission peaks separated by 245.2 ± 0.4 km s^{-1}. The mean emission line strengths, relative to the continuum, are $E/C = 1.132$ for the blue wing and $E/C = 1.125$ for the red wing. There is a slight linear decrease in E/C for the blue emission wing from $E/C = 1.15$ on JD 245 1499 to $E/C = 1.12$ 20 d later. The intensity of the bottom of the central absorption core is steady at $E/C = 0.941$. The ratio of the emission strengths of the blue (violet) to red intensities, as measured from the bottom of the central absorption, is $V/R = 1.047$.

In Fig. 10 we show the *V*/*R* ratio for Hα as a function of time for the SAAO and ESO data. A periodogram of these data shows that the most probable frequency is 0.42 cycles d^{-1} or its alias at 0.58 cycles d^{-1}, but almost nothing near the 1-d period. If the linear trend is removed, the most probable frequency remains at this value. A periodogram of the data with the linear trend removed is also shown in Fig. 10. We note that the period of the *V*/*R* variation is not significantly different from twice the photometric and spectroscopic period.

7 CONCLUSIONS

We have strong reasons to believe that ω Ori has a period of about $P = 0.970$ d for the light and line profile variations. An uncertain period of about 1 d for this star is mentioned by Peters & Gies (2000) from far-UV photometry, but no details are given. The line profile variation is characterized by an absorption feature which starts at the blue limb and moves to the red limb during half this period and moves from red to blue during the other half of the period. Another absorption feature moves in antiphase, indicating that two diametrically opposed clouds may be present. Conversely, this could also be interpreted as NRP with $|m| = 2$. The blue to red motion of the absorption feature indicates that it is seen over the pole and that the star is of low inclination.

We calculated some very crude simulations consisting of two areas on a uniform spherical photosphere where the width of the intrinsic line profile is slightly lower than in the photosphere. It is possible to reproduce the line profile variations seen in ω Ori without difficulty, but a unique solution cannot be found. The best models have an angle of inclination of about 30° and spot radii of about 20°. We cannot, on this basis alone, discriminate between this crude cloud model and NRP.

Our analysis of the line profiles leads to significantly lower values of the projected rotational velocity, $v \sin i$, for the helium lines relative to the metal lines. This cannot be because of different time-dependent line broadening of whatever origin, since the radial velocity amplitude of the helium lines is considerably smaller than the metal line amplitude. We interpret this to mean that the circumstellar material significantly contributes to the helium line formation, not only in He I 6678 and He I 5876 where overt emission is present in the wings, but also in the other helium lines.

We see the moving absorption subfeatures clearly in all the helium lines and also in Hβ. This indicates that the source of the periodic variability is present in the circumstellar material as well as in the photosphere. Evidence for this is very strong in other Be stars as well. In ζ Tau (Balona & Kaye 1999), the He I 6678 line has

the characteristic profile of a 'shell' line formed in the circumstellar material. In ϵ Cap (Balona & Lawson 2000), all helium line profiles are severely distorted by the circumstellar material. Yet in both stars the periodic moving absorption features are strongly seen in the difference profiles in all helium lines. In μ Cen (Balona et al. 2001), a strong moving absorption feature is seen not only in He I 6678, which displays strong line emission in the wings, but also in Hβ and Hα.

Since the periodic variations in Be stars seem to be associated with the circumstellar material, and the period in Be stars is not significantly different from the period of rotation (Balona 1990, 1995), we argue that the periodic variation is probably because of one or more clouds of circumstellar material corotating with the star. In this model, the period of rotation of ω Ori is the same as the period obtained here, $P = 0.970$ d. The radius of the star is not known with any accuracy, but from the spectral type and luminosity class we estimate it to be about $R/\mathrm{R}_\odot = 9 \pm 3$ for a B3 III star (see above). The above period then leads to an equatorial rotational velocity $v_\mathrm{e} = 470 \pm 150\,\mathrm{km\,s^{-1}}$. The angle of inclination is then somewhere between 20° and 40°. This agrees with the low angle of inclination implied by the over-the-pole motion of the absorption subfeature.

ACKNOWLEDGMENTS

The authors gratefully acknowledge the Director, and his staff, of the MSSSO for the generous allocation of telescope time and associated assistance. They also thank the staff of the Geneva observatory for the allocated time on the 1.2-m Euler telescope and for the use of the reduction software package for the CORALIE spectra. DJJ thanks the British Particle Physics and Astronomy Research Council for a post-doctoral research fellowship, and the Royal Society for a European research grant. DJJ would like to acknowledge the continued positive influences of Mrs J Pryer. ABK's work was performed under the auspices of the US Department of Energy by the Los Alamos National Laboratory under contract W-7405-ENG-36. Kitt Peak National Observatory is operated by the Association of Universities for Research in Astronomy, Inc. (AURA) under cooperative agreement with the National Science Foundation.

REFERENCES

Balona L. A., 1990, MNRAS, 245, 92
Balona L. A., 1995, MNRAS, 277, 1547
Balona L. A., 1999, MNRAS, 306, 407
Balona L. A., Lawson W. A., 2000, MNRAS, 321, 131
Balona L. A., Kaye A. B., 1999, ApJ, 521, 407
Balona L. A., Marang F., Monderen P., Reitermann A., Zickgraf F.-J., 1987, A&AS, 71, 11
Balona L. A., Cuypers J., Marang F., 1992, A&AS, 92, 533
Balona L. A., James D., Lawson W. A., Shobbrook R. R., 2001, MNRAS, 324, 1041
Ballereau D., Chauville J., Zorec J., 1995, A&AS, 111, 423
Baranne A. et al., 1996, A&AS, 119, 373
Gray R. O., Corbally C. J., 1994, AJ, 107, 742
Hillenbrand L. A., Strom S. E., Vrba F. J., Keene J., 1992, ApJ, 397, 613
Kovacs G., 1981, Ap&SS, 78, 175
Peters G., Gies D. R., 2000, in Smith M. A., Huib H., Fabregat J., eds, Proc. IAU Colloq. 175, The Be Phenomenon in Early-Type Stars, ASP Conf Ser. Vol. 214. Astron. Soc. Pac., San Franciso, p. 244
Porter J. M., 1996, MNRAS, 280, L31
Slettebak A., 1982, ApJS, 50, 55
Thé P. S., de Winter D., Pérez M. R., 1994, A&AS, 104, 315

This paper has been typeset from a TEX/LATEX file prepared by the author.